Hadron-quark transition and chiral symmetry restoration at high density

Hiroaki Kouno[1,*] and Kouji Kashiwa[2,†]

[1]*Department of Physics, Saga University, Saga 840-8502, Japan*
[2]*Fukuoka Institute of Technology, Wajiro, Fukuoka 811-0295, Japan*

A simple phenomenological hybrid hadron-quark model with excluded volume effects of baryons and chiral dynamics is investigated. The hybrid equation of state naturally connects the low-density baryonic matter with the high-density quark matter. In the intermediate region, a phase, which cannot be regarded as pure hadron matter or pure quark matter, appears. In this model, there is a possibility that the abrupt first-order-like transition to pure quark matter induces the strong chiral symmetry restoration and the speed of sound has a large peak at considerable large density.

I. INTRODUCTION

Exploration of the QCD phase diagram is an important subject not only in particle and nuclear physics but also in astrophysics and cosmology; for a review, see, e.g., Ref. [1] and references therein. However, at finite baryon (or quark) chemical potential, the first principle calculation, i.e., the lattice QCD simulation, is not feasible due to the infamous sign problem. To avoid the problem, several methods are proposed and investigated, but, at present, these methods are not complete, and we do not have the established equation of state (EOS) at finite baryon density.

At low temperature, there is nuclear (baryonic) matter at saturation density. As the density increases, other baryons may appear. At the extreme high density, the chiral symmetric quark matter is expected to appear and conformality is restored. However, at present, we do not have a definite information of the EOS in the intermediate region between the saturation density and the extremely high density.

It is known that repulsive effects among baryons are important in the intermediate region. If repulsion is absent, then the baryonic matter is realized at sufficiently large baryon density [2]. One of the traditional treatments of such repulsion is to consider the excluded volume effects (EVE) among baryons [3–5]. The excluded volume effects successfully prevent baryonic matter from realizing at

sufficiently large baryon density; for a recent review, see, e.g., Ref. [6] and references therein.

At large density, the chiral symmetry restoration is also expected. The Nambu–Jona-Lasinio (NJL) model [7] is a simple but very useful model to describe the restoration; as a review, see, e.g., Ref. [8] and references therein. However, the NJL model cannot describe the hadron-quark transition.

Furthermore, recently, it has been emphasized that the trace anomaly and the speed of sound are very important to understand the properties of the high density hadron and quark matter; see, e.g., Refs. [9,10] and references therein.

In this paper, we construct a simple phenomenological hybrid hadron-quark model with EVE of baryons and chiral dynamics. The model naturally connects the baryonic matter at low density and the quark matter at high density. It can also describe the chiral restoration. It is found that, in this hybrid model, there is a possibility that the abrupt first-order like transition to pure quark matter induces the strong restoration of chiral symmetry and the speed of sound has a large peak.

This paper is organized as follows. In Sec. II, the hybrid model is formulated. In Sec. III, numerical results are shown for two typical cases. Section IV is devoted to a summary and discussion.

II. FORMALISM

First, we give a sketch of our strategy of calculations. Our main purpose is to know the μ_B dependence of the thermodynamic quantities of hadron or quark matter, where μ_B is the baryon chemical potential. First, we construct the baryon number density n_B with the EVE of baryons. Next we require that n_B approaches $\frac{n_q}{3}$ in the high density limit, where n_q is the quark number density of pure quark phase. In this procedure, n_B depends on the chiral condensates σ_f ($f = u, d, s$) that are included in the quark model. Using the

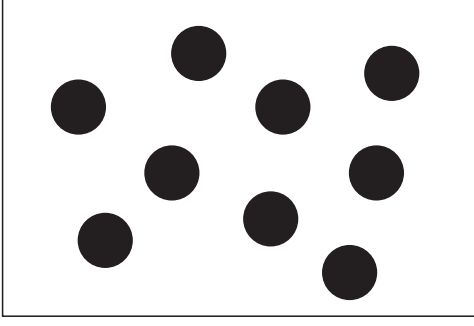*kounoh@cc.saga-u.ac.jp
†kashiwa@fit.ac.jp

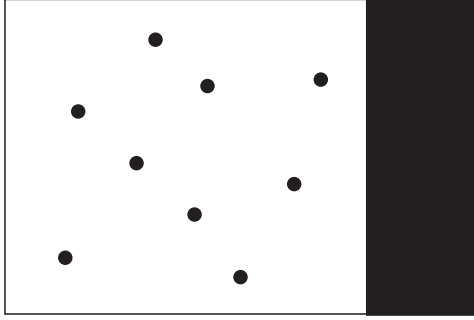FIG. 1. Schematic figure of N nonpointlike baryons in the system with volume V.

FIG. 2. Schematic figure of N pointlike baryons in the system with effective volume $V - v_{\mathrm{B}}N$. The volume of the dark region is $v_{\mathrm{B}}N$.

thermodynamic equation, the σ_f dependence of the thermodynamic potential density $\Omega \, (= -P)$ is obtained, where P is the pressure of the system. The values of σ_f are determined to minimize Ω (or maximize P). Using the obtained values of σ_f, the other thermodynamic quantities are calculated.

As shown in Fig. 1, we consider N nonpointlike baryons in the system with volume V where N is the number of baryons. We consider this system to be equivalent to the system of N pointlike baryons in the effective volume $V - v_{\mathrm{B}}N$, where v_{B} is the volume of a baryon, see Fig. 2. Then, the following equation is satisfied:

$$\tilde{n}_{\mathrm{B}} = \frac{N}{V - v_{\mathrm{B}}N} = \frac{n_{\mathrm{B}}}{1 - v_{\mathrm{B}}n_{\mathrm{B}}}, \qquad (1)$$

where $n_{\mathrm{B}} = \frac{N}{V}$ is the baryon density of nonpointlike baryon and $\tilde{n}_{\mathrm{B}}$ is the one of N pointlike baryons. In this paper, we add a tilde to the baryon number density of pointlike baryons. Hence, the baryon number density of baryonic matter with EVE is given by

$$n_{\mathrm{B}} = \frac{\tilde{n}_{\mathrm{B}}}{1 + v_{\mathrm{B}}\tilde{n}_{\mathrm{B}}} < \frac{1}{v_{\mathrm{B}}}. \qquad (2)$$

The pressure P of the baryonic matter with the excluded volume effects is determined by the thermodynamic equation

$$\frac{\partial P(T, \mu_{\mathrm{B}})}{\partial \mu_{\mathrm{B}}} = n_{\mathrm{B}}. \qquad (3)$$

The other thermodynamic quantity, such as the energy density ε, is determined by the thermodynamic relation. Hereafter, we concentrate on EOS at zero temperature and omit the variable T for simplicity. Then, Eq. (3) is represented as $\frac{dP}{d\mu_{\mathrm{B}}}$.

When a constant v_{B} is used, the speed of sound,

$$c_{\mathrm{Bs}} = \sqrt{\frac{dP_{\mathrm{B}}}{d\varepsilon_{\mathrm{B}}}} = \sqrt{\frac{dP_{\mathrm{B}}}{d\mu_{\mathrm{B}}} \Big/ \frac{d\varepsilon_{\mathrm{B}}}{d\mu_{\mathrm{B}}}}, \qquad (4)$$

may exceed the speed of light $c \, (= 1)$ and the causality can be easily violated. In fact, when $v_{\mathrm{B}}\tilde{n}_{\mathrm{B}} \gg 1$, we have

$$\frac{dP_{\mathrm{B}}}{d\mu_{\mathrm{B}}} = n_{\mathrm{B}} = \frac{\tilde{n}_{\mathrm{B}}}{1 + v_B \tilde{n}_{\mathrm{B}}} \sim \frac{1}{v_{\mathrm{B}}}, \qquad (5)$$

$$\frac{d\varepsilon_{\mathrm{B}}}{d\mu_{\mathrm{B}}} = \frac{d}{d\mu_{\mathrm{B}}}(\mu_{\mathrm{B}}n_{\mathrm{B}} - P_{\mathrm{B}}) = \mu_{\mathrm{B}}\frac{dn_{\mathrm{B}}}{d\mu_{\mathrm{B}}} \sim 0. \qquad (6)$$

This means that the EOS becomes very hard and the speed of sound diverges. Therefore, the density dependence of v_{B} is very important.

It is natural to assume that the baryon number of the system approaches the one of the pure quark system with the same chemical potential, when the baryon chemical potential is very large. This requirement can be achieved if we assume

$$v_{\mathrm{B}} = \frac{3}{n_{\mathrm{q}}} \quad (n_{\mathrm{q}} \neq 0), \qquad (7)$$

where n_{q} is the quark number density of the pure quark matter. In other words, we assume that the EOS inside the baryons is described by the pure-quark model. The baryon number density is given by

$$n_{\mathrm{B}} = \frac{\tilde{n}_{\mathrm{B}}}{1 + v_{\mathrm{B}}\tilde{n}_{\mathrm{B}}}, \qquad (8)$$

$$= \frac{n_{\mathrm{q}}\tilde{n}_{\mathrm{B}}}{n_{\mathrm{q}} + 3\tilde{n}_{\mathrm{B}}} < \frac{n_{\mathrm{q}}}{3}. \qquad (9)$$

Hence, the EOS is expected to approach the pure quark EOS at high density. When $3\tilde{n}_{\mathrm{B}} \gg n_{\mathrm{q}}$, we obtain

$$n_{\mathrm{B}} \sim \frac{n_{\mathrm{q}}}{3}. \qquad (10)$$

When $n_{\mathrm{q}} \neq 0$ and $\tilde{n}_{\mathrm{B}} \neq 0$, Eq. (9) can be rewritten as

$$n_{\mathrm{B}} = \frac{\frac{1}{3}n_{\mathrm{q}}}{1 + v_{\mathrm{q}}n_{\mathrm{q}}}, \qquad (11)$$

FIG. 3. Schematic figure of $3N$ quarks in the system with effective volume $v_\mathrm{B}N$. The volume of the dark region is $3v_\mathrm{q}N$.

$$= \frac{1}{v_\mathrm{B} + 3v_\mathrm{q}}, \tag{12}$$

$$= \frac{1}{3}\left(\frac{1}{n_\mathrm{q}} + \frac{1}{3\tilde{n}_\mathrm{B}}\right)^{-1}, \tag{13}$$

where $v_\mathrm{q} = \frac{1}{3\tilde{n}_\mathrm{B}}$. From Eq. (11), we see that the system can also be regarded as the matter of quarks with finite effective volume v_q, see Fig. 3. In this sense, this model has a quark-hadron duality; for a general review of quark-hadron duality, see, e.g., Ref. [11] and references therein. It is also interesting that Eq. (13) resembles the law of combined resistance of parallel resistances. The large v_B causes the strong suppression of baryonic matter. When $3v_\mathrm{q} < v_\mathrm{B}$, it is natural to regard that the system is composed of quarks with small volume v_q rather than baryons with large volume v_B.

However, when $n_\mathrm{q} = 0$, v_B cannot be defined. On the other side, it is known that, below the saturation density, the nucleon has a finite volume $v_\mathrm{B0} = \frac{4\pi r_\mathrm{B0}^3}{3}$ with the nucleon radius $r_\mathrm{B0} = 0.8$ fm. Hence, we interpolate between v_B0 and $\frac{3}{n_\mathrm{q}}$ with the following smooth function of n_q:

$$v_\mathrm{B} = \frac{3}{n_\mathrm{q}'}, \tag{14}$$

with

$$n_\mathrm{q}' = n_\mathrm{q} + \frac{3}{v_\mathrm{B0}}\exp\left[-a\left(\frac{v_\mathrm{B0}n_\mathrm{q}}{3}\right)^2\right], \tag{15}$$

where a is a free parameter and controls how abruptly v_B approaches $3/n_\mathrm{q}$. Note that, as is shown below, n_q depends on chiral condensates in our model. Hence, v_B and n_B also depend on the chiral condensates.

For the pointlike hadron model, we use the hadron resonance gas (HRG) model. The number density is given as

$$\tilde{n}_\mathrm{B} = \sum_{i=\mathrm{Baryon}} n_\mathrm{IFG}(g_{\mathrm{B}i}, m_{\mathrm{B}i}, \mu_\mathrm{B}), \tag{16}$$

where $g_{\mathrm{B}i}$ and $m_{\mathrm{B}i}$ are the spin degeneracy and the mass of ith baryon, respectively. The function $n(g, m, \mu)$ is the number density of ideal fermion gas with the degeneracy factor g, the mass m, and the chemical potential μ at zero temperature, and is given by

$$n_\mathrm{IFG}(g, m, \mu) = \begin{cases} 0 & (\mu < m) \\ \frac{g}{6\pi^2}(\mu^2 - m^2)^{3/2} & (\mu \geq m) \end{cases}. \tag{17}$$

In this paper, for simplicity, we use the same v_B for all baryons.

For pure quark matter, we use the three-flavor NJL model with mean field approximation. The quark number density of the NJL model is given by

$$n_\mathrm{q} = \sum_{f=u,d,s} n_\mathrm{IFG}(6, M_f, \mu_\mathrm{q}), \tag{18}$$

where M_f and $\mu_\mathrm{q}(= \mu_\mathrm{B}/3)$ are the effective mass of f quark and the quark chemical potential, respectively. The effective quark mass is given by

$$M_f = m_f - 4G_\mathrm{s}\sigma_f + 2G_\mathrm{d}\sigma_f'\sigma_f'', \tag{19}$$

with $f \neq f'$, $f \neq f''$, and $f' \neq f''$, where m_f is the current quark mass of f quark, G_s and G_d are coupling constants of four and six-quarks interaction, and σ_f is the chiral condensate of f quark, respectively. In the pure quark system, the pressure is given by

$$P = P_\mathrm{v} + P_{D,\mathrm{NJL}} - U_\mathrm{m}, \tag{20}$$

where P_v, U_m, and $P_{D,\mathrm{NJL}}$ are the Dirac sea contributions, the mesonic and the density parts of the NJL model, respectively. For each flavor, the density part $P_{D,\mathrm{NJL}}$ is given by $P_\mathrm{F}(M_f, \mu_\mathrm{q})$, which is equivalent to the pressure of the free quark gas with the quark mass M_f and the quark chemical potential μ_q. The Dirac sea contributions are given by

$$P_\mathrm{v}(M_f) = -\sum_{f=u,d,s} \frac{M_f^4}{4\pi^2}\left[\left(\frac{E_{\mathrm{v}f}\Lambda}{M_f^2}\right)\left(\frac{E_f^2}{M_f^2} - \frac{5}{2}\right) + \frac{3}{2}\log\left(\frac{E_{\mathrm{v}f} + \Lambda}{M_f}\right)\right], \tag{21}$$

where $E_{\mathrm{v}f} = \sqrt{\Lambda^2 + M_f^2}$ with the three dimensional momentum cutoff Λ. The Dirac sea contributions have no explicit μ_q dependence. However, P_v depends on μ_q, since M_f depends on μ_q. The mesonic part is given by

$$U_\mathrm{m} = 2G_\mathrm{s}(\sigma_u^2 + \sigma_d^2 + \sigma_s^2) - 4G_\mathrm{d}\sigma_u\sigma_d\sigma_s. \tag{22}$$

According to Ref. [12], we set $m_{u,d} = 5.5$ MeV, $m_s = 140.7$ MeV, $G_s\Lambda^2 = 1.835$, $G_d\lambda^5 = 12.36$, and $\Lambda = 602.3$ MeV.

Instead of Eq. (20), in the hybrid model, the total pressure P of the system is given by

$$P = P_v + P_D - U_m. \qquad (23)$$

Using n_B given by Eq. (2) with Eq. (14), the density part P_D is given by

$$P_D(\mu_B, \sigma_f) = \int_0^{\mu_B} d\mu\, n_B(\mu, \sigma_f), \qquad (24)$$

where the integration is performed with fixing all σ_f so as to satisfy the relation

$$\left.\frac{\partial P(\mu_B, \sigma_f)}{\partial \mu_B}\right|_{\sigma_f\text{fixed}} = n_B(\mu_B, \sigma_f). \qquad (25)$$

The value of the chiral condensate σ_f is determined to maximize P and satisfy

$$\frac{\partial P(\mu_B, \sigma_f)}{\partial \sigma_f} = 0. \qquad (26)$$

Hence, the thermodynamic relation

$$\begin{aligned}
\frac{dP(\mu_B, \sigma_f(\mu_B))}{d\mu_B} &= \left.\frac{\partial P}{\partial \mu_B}\right|_{\sigma_f\text{fixed}} + \sum_{f=u,d,s}\frac{\partial P}{\partial \sigma_f}\frac{d\sigma_f}{\mu_B}, \\
&= \left.\frac{\partial P_D}{\partial \mu_B}\right|_{\sigma_f\text{fixed}}, \\
&= n_B(\mu_B, \sigma_f(\mu_B)), \qquad (27)
\end{aligned}$$

is satisfied. Therefore, using Eq. (24), once P_D is obtained as the function of σ_f and the solution σ_f which maximizes the total pressure (23) is determined, the equation of motion (26) and the thermodynamic relation (27) are automatically satisfied. The energy density ε of the total system is determined using the thermodynamic relation

$$\varepsilon = \mu_B n_B - P. \qquad (28)$$

Following the above procedure, the quark and hadron matters are correlated with each other in the level of the pressure via EVE. This is also true for the thermodynamic potential density Ω because there is a direct relation to the pressure, namely $\Omega = -P$. The functional form of $\Omega(\sigma_f)$ deviates largely from the one $\Omega_{NJL}(\sigma_f)$ in the original NJL model in the intermediate region of μ_B. Therefore, our result can provide the crossover behavior even if the NJL model itself has the first-order chiral transition at low T in the moderately high density region; since the

thermodynamic potential is deformed by the hadron contributions, they act as the external term that explicitly breaks chiral symmetry.

The hybrid model approaches in the NJL model in the high density limit. As is seen in the next section, when n_B approaches $\frac{n_q}{3}$ gradually, crossover chiral transition takes place. When n_B approaches $\frac{n_q}{3}$ abruptly, first-order-like transition happens.

The original NJL model has a cutoff. However, at zero temperature, the chemical potential is the natural cutoff for energy and momentum. Hence, in the numerical calculations, we use the cutoff only in the Dirac sea contributions. In this procedure, the physical quantities are expected to approach those in the free quark gas model. In the HRG part, we include all baryons listed in the list of Particle Data Group [13], but they only contribute to the results when their masses are smaller than the baryon chemical potential μ_B.

Several hybrid models have been already proposed. For example, in Ref. [14], the hyperbolic functions are used as an interpolation function of EOS. In our model, we do not give such an interpolation function but give a more microscopic quantity, namely, the density dependence of baryon volume in EVE. In Ref. [15], the hybrid model based on quarkyonic matter and the EVE is investigated. In our model, we do not assume quarkyonic matter, but some kind of more macroscopic quark-hadron duality (11) is assumed. The macroscopic model may be simpler and more convenient than the microscopic one, but it has a less dynamical description. The study of the relation between several hybrid models is an important problem in the future.

III. NUMERICAL RESULTS

Our hybrid model has one free parameter a in Eq. (15). In this section, we show the numerical results in two typical cases, a crossover transition ($a = 0.1$) and a first-order-like transition ($a = 0.8$). Hereafter, we use the quark chemical potential $\mu_q = \frac{\mu_B}{3}$ instead of μ_B since we are interested in the chiral dynamics of quarks as well as the hadron-quark transition.

The numerical calculations are done according to the following procedures:

(1) For given μ_B, $\tilde{n}_B$ is calculated using the HRG model.

(2) For fixed value of σ_f, n_q is calculated.

(3) Using $\tilde{n}_B$ and n_q as inputs, n_B is calculated as an output.

(4) Using Eq. (24) and n_B, Ω ($= -P$) is calculated for the fixed value of σ_f.

(5) Changing the value of σ_f and doing the same calculation as the procedure (2) $\sim$ (4), a functional form $\Omega(\sigma_f)$ ($= -P(\sigma_f)$) is determined.

(6) Determine the solution σ_f which minimizes Ω (maximizes P).

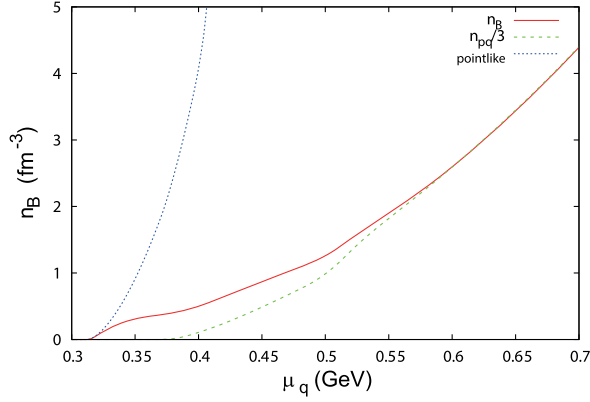(7) Using the obtained solution σ_f, the other quantities are calculated as well as P and n_B.

FIG. 4.   The μ_q dependence of the baryon number density n_B with the crossover setup. The solid, dashed, and dotted lines show n_B, $\frac{n_q}{3}$ and $\tilde{n}_B$ (pointlike), respectively.

Note that the equation of motion (26) and the thermodynamic relation (27) are automatically satisfied by minimizing (maximizing) Ω (P).

A. Crossover transition

First, we show the results with $a = 0.1$; in the following, we call it the crossover setup. Figure 4 shows the μ_q dependence of the baryon number density n_B. Note that not only n_B but also n_q depends on the values of the chiral condensates determined in the framework of the hybrid model. We see that n_B coincides with $\tilde{n}_B$ at low density and, at $\mu_q \sim 0.33$ GeV, begins to deviate from $\tilde{n}_B$. As μ_q increases, n_B approaches $\frac{n_q}{3}$ smoothly. Although the hadron-quark transition is a smooth crossover, we can regard the system as in the quark phase when $\mu_q > 0.55$ GeV. In the intermediate region $\mu_q = 0.33$–0.55 GeV, it is difficult to identify the system as pure hadron matter or pure quark matter.
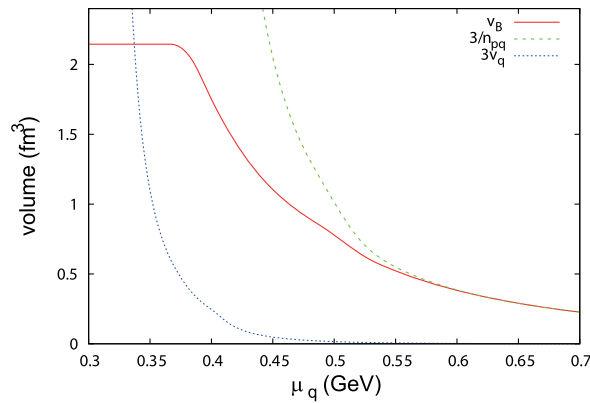
FIG. 5.   The μ_q dependence of the baryon volume v_B with the crossover setup. The solid, dashed, and dotted lines show v_B, $\frac{3}{n_q}$, and $3v_q$, respectively.

Figure 5 shows the μ_q dependence of the baryon volume v_B. We see that v_B approaches $3/n_q$ smoothly as μ_q increases. When $\mu_q > 0.35$ GeV, $3v_q$ is smaller than v_B. Hence we may regard the system to be composed of quarks rather than baryons when $\mu_q > 0.35$ GeV.

Figure 6 shows the μ_q dependence of the effective quark mass M_f. We see that M_f starts to decrease when μ_q exceeds the value of the effective light-quark mass at vacuum and gradually decreases as μ_q increases. M_f somewhat decreases early when μ_q exceeds 0.5 GeV. Comparing Figs. 5 and 6, we see that M_f decreases early when $3v_q$ is negligible.

With the crossover setup, the hybrid model approaches the NJL model gradually as μ_q increases. Figure 7 shows the σ_l ($l = u, d$) dependence of the thermodynamic potential Ω. We see that the value of $|\sigma_l|$ in the minimum of Ω decreases only slowly.
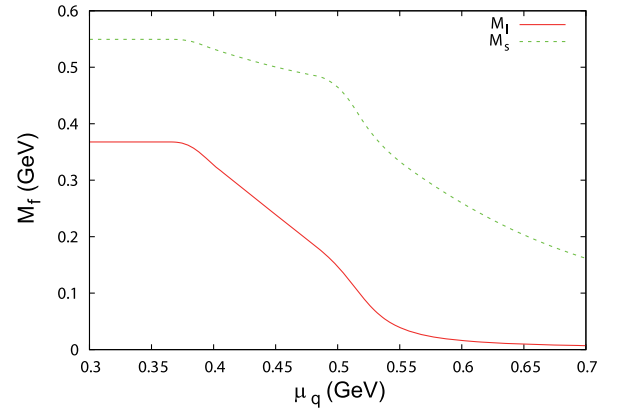

FIG. 6.   The μ_q dependence of the effective quark mass M_f with the crossover setup. The solid and dashed lines show M_l ($l = u, d$) and M_s, respectively.
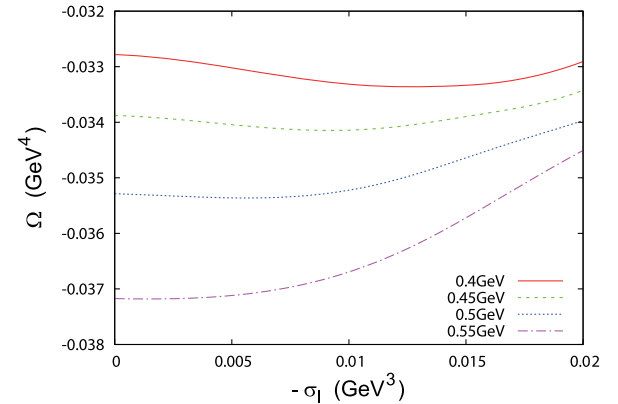

FIG. 7.   The σ_l dependence of the thermodynamic potential Ω with the crossover setup. The solid, dashed, dotted, and dot-dashed lines show the results at $\mu_q = 0.4$, 0.45, 0.5, and 0.55 GeV, respectively. For each case, the value of σ_s is fixed to the value in the minimum of $\Omega(\sigma_f)$.
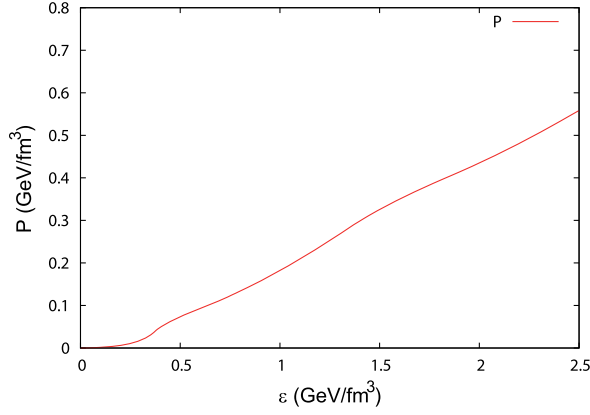
FIG. 8. The relation between the energy density ε and the pressure P in our hybrid model with the crossover setup.

Figure 8 shows the ε-P relation. Since ε and P have the Dirac sea contributions which are not zero even at $\mu_q = 0$, we subtract $\varepsilon(\mu_q = 0)$ and $P(\mu_q = 0)$ from ε and P, respectively. We see that P increases monotonically as ε increases. The intermediate phase mentioned above exists in the region $\varepsilon = 0.2$–2.5 GeV/fm^3.

According to Ref. [9], we introduce the following quantities:

$$\eta = \log\left(\frac{\varepsilon}{\varepsilon_0}\right), \tag{29}$$

where $\varepsilon_0 = 0.15$ GeV/fm^3, and

$$\Delta = \frac{1}{3} - \frac{P}{\varepsilon}. \tag{30}$$

When Δ vanishes, the trace anomaly $\varepsilon - 3P$ becomes zero and the conformality is expected to be hold. Figure 9 shows the μ_q dependence of η. η increases monotonically as μ_q increases. The intermediate region $\mu_q = 0.33$–0.55 GeV
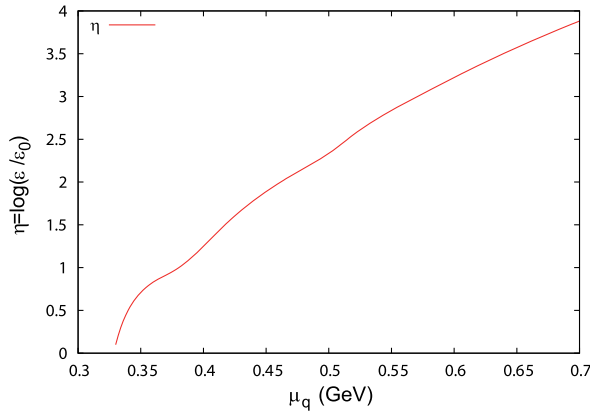
FIG. 9. The μ_q dependence of η obtained by using our hybrid model with the crossover setup.
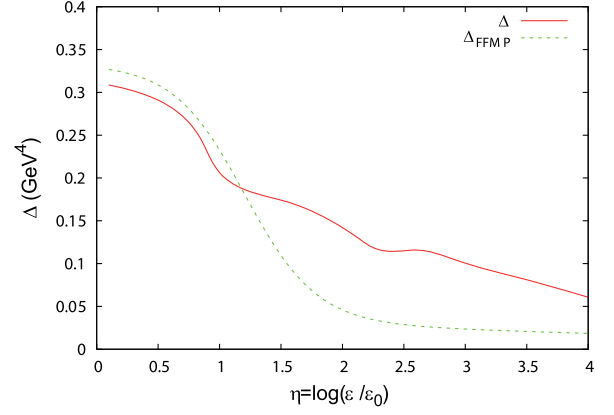

FIG. 10. The η dependence of Δ with the crossover setup. The solid and dashed lines show the result of our hybrid model and the result obtained by parametrization (7) in Ref. [9], respectively.

corresponds to the region $\eta = 0.1 \sim 2.8$. The solid line in Fig. 10 shows the η dependence of Δ obtained by our hybrid model. The dashed line shows the result obtained by parametrization in Ref. [9],

$$\Delta = \frac{1}{3} - \frac{1}{3} \cdot \frac{1}{e^{-\kappa(\eta - \eta_c)} + 1}\left(1 - \frac{A}{B + \eta^2}\right), \tag{31}$$

where $\kappa = 3.45$, $\eta_c = 1.2$, $A = 2$, and $B = 20$. In this paper, we call this parametrization Δ_{FFMP}. Our result Δ is in good agreement with Δ_{FFMP} when $\eta < 1$, but somewhat deviates from Δ_{FFMP} at large η.

Using Δ and η, the square of the speed of sound c_s^2 is rewritten as [9]

$$c_s^2 = \frac{dP}{d\varepsilon} = c_{s,,d}^2 + c_{s,\text{nd}}^2, \tag{32}$$

where the derivative and nonderivative parts are given by

$$c_{s,d}^2 = -\frac{d\Delta}{d\eta}, \qquad c_{s,nd}^2 = \frac{1}{3} - \Delta = \frac{P}{\varepsilon}. \tag{33}$$

Figure 11 shows the η dependence of c_s^2. c_s^2 has a double peak structure and, in the region $\eta = 0.7 \sim 3$, somewhat deviates from the parametrization result. The left peak is higher than the right one. It seems that the left peak is induced by the repulsion forces (i.e., excluded volume effects) among baryons, and the right one is related to the hadron-quark transition and the enhancement of the chiral symmetry restoration. It seems that this structure of c_s^2 corresponds to the right sketch in Fig. 2 in Ref. [10]. Figure 12 shows the η dependence of $c_{s,d}^2$ and $c_{s,\text{nd}}^2$. It seems that the double peaks are originated in the derivative part. At large η, $c_{s,d}^2$, and $c_{s,\text{nd}}^2$ somewhat deviate from the parametrization results, but the deviations cancel each
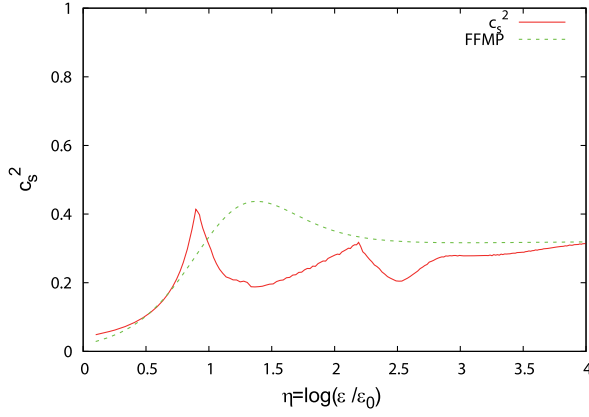
FIG. 11.   The η dependence of c_s^2 with the crossover setup. The solid and dashed lines show the result of our hybrid model and the result obtained by parametrization (7) in Ref. [9], respectively.
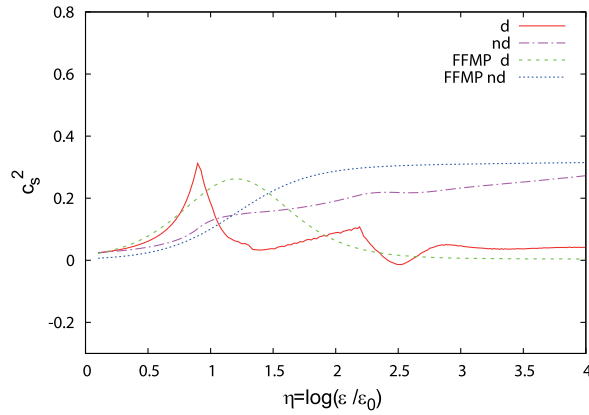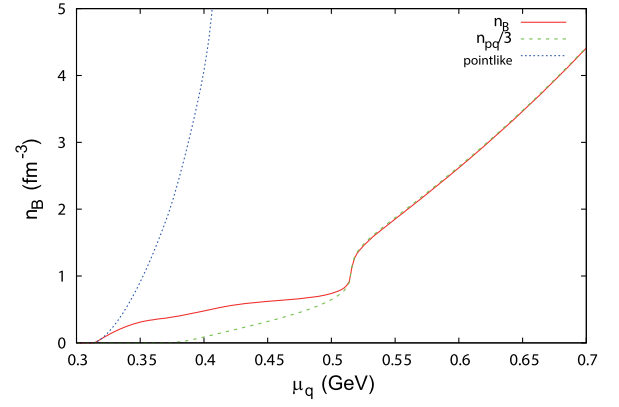

FIG. 13.   The μ_q dependence of the baryon number density n_B with the first-order-like setup. The solid, dashed, and dotted lines show n_B, $\frac{n_q}{3}$, and $\tilde{n}_B$ (pointlike), respectively.
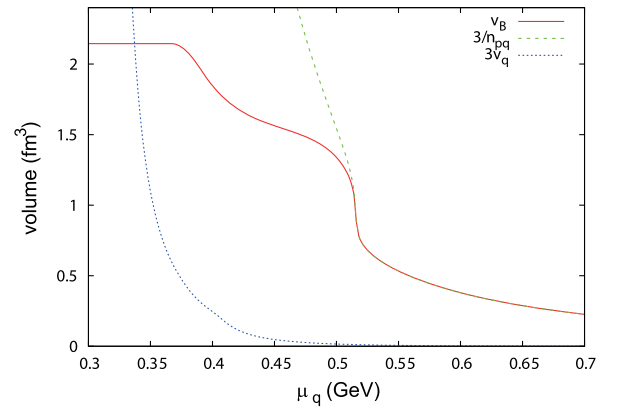

FIG. 12.   The η dependence $c_{s,d}^2$ and $c_{s,nd}^2$ with the crossover setup. The solid and dash-dotted lines show $c_{s,d}^2$ and $c_{s,nd}^2$ in our hybrid model, respectively. The dashed and dotted lines show $c_{s,d}^2$ and $c_{s,nd}^2$ obtained by parametrization (7) in Ref. [9], respectively.

FIG. 14.   The μ_q dependence of the baryon volume v_B with the first-order-like setup. The solid, dashed, and dotted lines show v_B, $\frac{3}{n_q}$, and $3v_q$, respectively.

other, and the total c_s^2 is in good agreement with the parametrization.

B. First-order-like transition

Next, we show the results with $a = 0.8$; in the following, we call it the first-order-like setup. Figure 13 shows the μ_q dependence of the baryon number density n_B. We can see that n_B coincides with $\tilde{n}_B$ at low density. As μ_q increases, n_B approaches $\frac{n_q}{3}$. Finally, n_B coincides with $\frac{n_q}{3}$ at $\mu_q = 0.52$ GeV, and increases rapidly. In this case, it seems that the first-order-like transition occurs at $\mu_q = 0.52$ GeV. It is clear that the system is in a pure quark phase when $\mu_q > 0.52$ GeV. However, it seems that the system is in the intermediate phase rather than in the hadron phase in the region $\mu_q = 0.33$–0.52 GeV.

Figure 14 shows the μ_q dependence of the baryon volume v_B. We see that v_B coincides with $3/n_q$ at

$\mu_q = 0.52$ GeV and decreases rapidly. When $\mu_q > 0.35$ GeV, $3v_q$ is smaller than v_B. Hence, it is natural to regard that the system is composed of quarks rather than baryons even when $\mu_q = 0.35$–0.52 GeV, although it is not in the pure quark phase.

Figure 15 shows the μ_q dependence of the effective quark mass M_f. We see that M_f starts to decrease when μ_q exceeds the value of the effective light quark mass at vacuum, gradually decreases as μ_q increases, and then has an abrupt decrease at $\mu_q = 0.52$ GeV. The abrupt restoration of the chiral symmetry occurs at $\mu_q = 0.52$ GeV. It seems that this abrupt restoration of chiral symmetry is related to the abrupt increase of n_B. It is known that in an abrupt transition, different physical quantities are correlated to each other near the transition point [16–18]. Hence, in this hybrid model, the abrupt changes in n_B and M_f are correlated with each other.
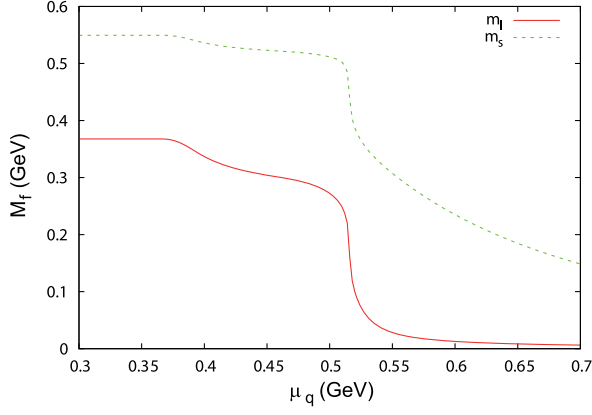
FIG. 15. The μ_q dependence of the effective quark mass M_f with the first-order-like setup. The solid and dashed lines show $M_l(l = u, d)$ and M_s, respectively.
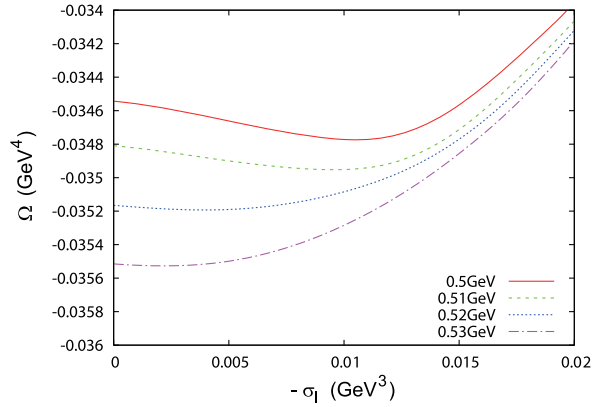

FIG. 17. The relation between the energy density ε and the pressure P in our hybrid model with the first-order-like setup.

FIG. 16. The σ_l dependence of the thermodynamic potential Ω with the first-order-like setup. The solid, dashed, dotted, and dot-dashed lines show the results at $\mu_q = 0.5$, 0.51, 0.52, and 0.53 GeV, respectively. For each case, the value of σ_s is fixed to the value in the minimum of $\Omega(\sigma_f)$.

FIG. 18. The μ_q dependence of η in our hybrid model with the first-order-like setup.

With the first-order-like setup, the hybrid model approaches the NJL model abruptly as μ_q increases. Figure 16 shows the σ_l dependence of the thermodynamic potential Ω. We see that the value of $|\sigma_l|$ in the minimum of Ω decreases rapidly. It should be noted that the bottom of Ω is almost flat at $\mu_q = 0.52$ GeV.

Figure 17 shows the $\varepsilon - P$ relation. We see that P increases monotonically as ε increases when $\varepsilon > 1$ GeV/fm^3 or $\varepsilon < 1.5$ GeV/fm^3. There is a plateau of P in the region $\varepsilon = 1$–1.5 GeV/fm^3. This plateau is induced by the first-order-like transition. The intermediate phase exists in the region $\varepsilon = 0.2$–1.8 GeV/fm^3.

Figure 18 shows the μ_q dependence of η. There is the tendency that η increases monotonically as μ_q increases and has an abrupt increase at $\mu_q = 0.52$ GeV. The intermediate region $\mu_q = 0.33$–0.52 GeV corresponds to the region $\eta = 0.1 \sim 2$.
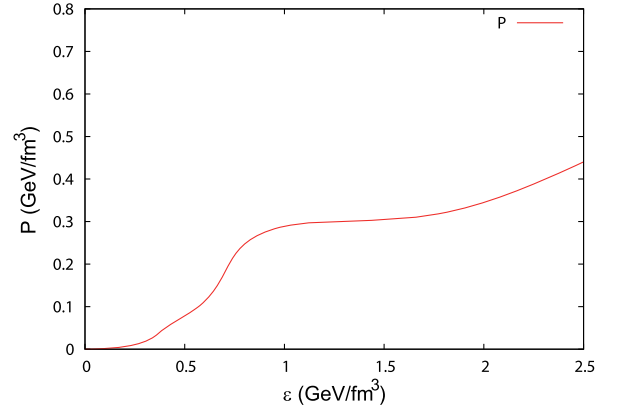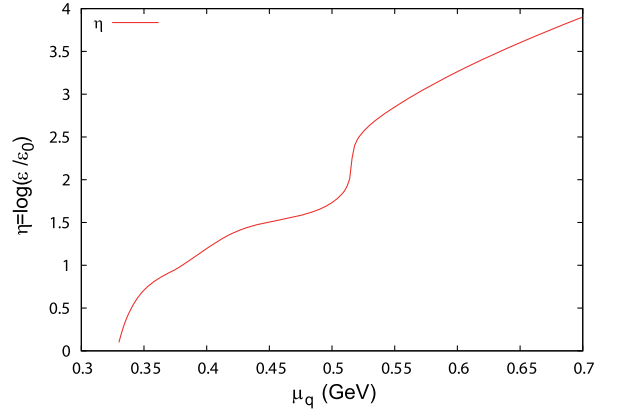
The solid line in Fig. 19 shows the η dependence of Δ in our hybrid model. Our result of Δ is in good agreement with Δ_{FFMP}, where Δ_{FFMP} means the result obtained by parametrization (7) in Ref. [9], when $\eta < 1.5$, but somewhat deviate from Δ_{FFMP} at large η.

Figure 20 shows the η dependence of c_s^2. We can see that c_s^2 has a double peak structure and, in the region $\eta = 0.7 \sim 3$, somewhat deviates from the parametrization result. In contrast to Fig. 11, the right peak is higher than the left one. It seems that the left peak is induced by the repulsion forces among baryons and that the right peak is related to the hadron-quark transition and the chiral symmetry restoration. Figure 21 shows the η dependence of $c_{s,d}^2$ and $c_{s,nd}^2$. It seems that the double peaks are originated in the derivative part. As in the case of Fig. 12, $c_{s,d}^2$ and $c_{s,nd}^2$ somewhat deviate from parametrization results at large η, but the deviations cancel each other and the total c_s^2 is in good agreement with the parametrization. It seems that this structure of c_s^2 corresponds to the left sketch in Fig. 2 in Ref. [10].
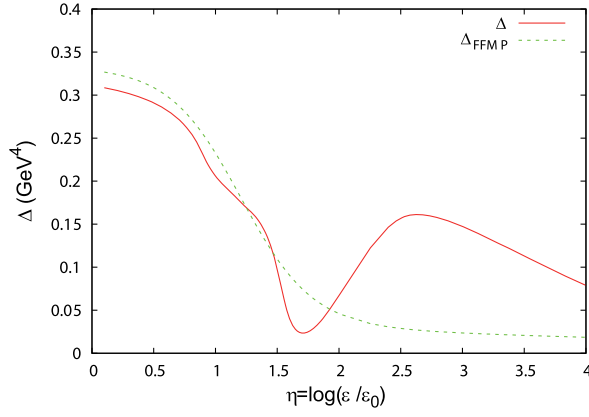
FIG. 19.　The η dependence of Δ with the first-order-like setup. The solid and dashed lines show the result of our hybrid model and the result obtained by parametrization (7) in Ref. [9], respectively.
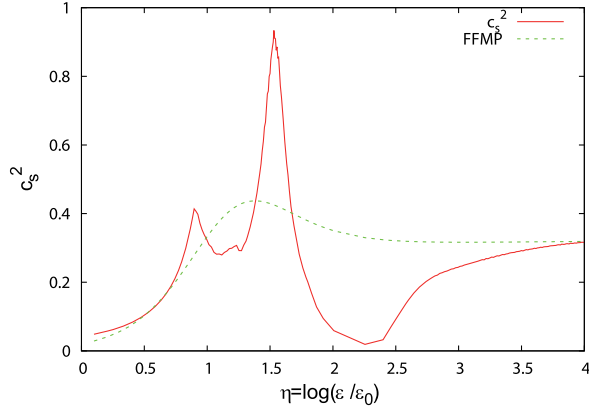

FIG. 20.　The η dependence of c_s^2 with the first-order-like setup. The solid and dashed lines show the result of our hybrid model and the result obtained by parametrization (7) in Ref. [9], respectively.
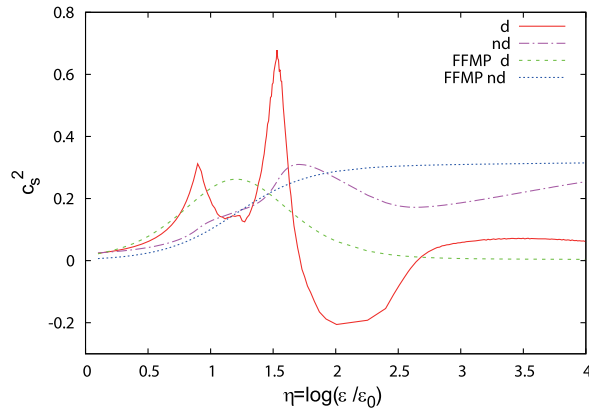

FIG. 21.　The η dependence $c_{s,\mathrm{d}}^2$ and $c_{s,nd}^2$ with the first-order-like setup. The solid and dash-dotted lines show $c_{s,\mathrm{d}}^2$ and $c_{s,\mathrm{nd}}^2$ in our hybrid model, respectively. The dashed and dotted lines show $c_{s,\mathrm{d}}^2$ and $c_{s,\mathrm{nd}}^2$ obtained by parametrization (7) in Ref. [9], respectively.

It should be noted that the baryon number density has one to one correspondence to the other thermodynamic quantities since we only use the thermodynamic relations to calculate these quantities. Hence, the μ_q dependence of the baryon number density is strongly correlated with the μ_q dependence of the other thermodynamic quantities. Figure 22 shows the μ_q dependence of the baryon number density when the baryon volume

$$v_\mathrm{B} = \frac{3}{n_\mathrm{q}'}, \qquad (34)$$

with

$$n_\mathrm{q}' = n_\mathrm{q} + \frac{3}{v_{\mathrm{B}0}} \exp\left[-3\left(\frac{v_{\mathrm{B}0}(n_\mathrm{q} + n_\mathrm{q}^3)}{6}\right)^2\right], \quad (35)$$

is used instead of Eq. (14). Figure 22 resembles Fig. 13. Figure 23 shows the η dependence of the speed of sound.
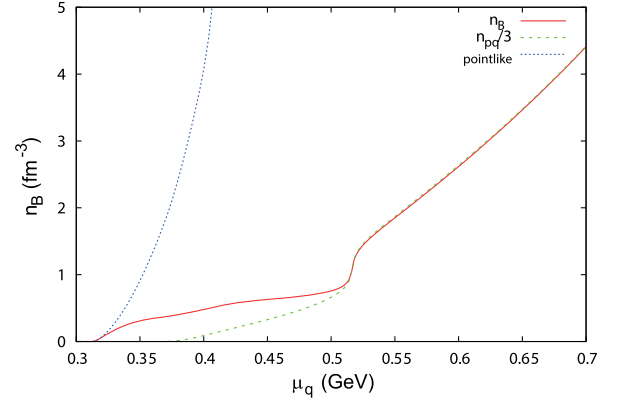

FIG. 22.　The μ_q dependence of the baryon number density n_B with the baryon volume (34). The solid, dashed, and dotted lines show n_B, $\frac{n_\mathrm{q}}{3}$ and $\tilde{n}_\mathrm{B}$ (pointlike), respectively.
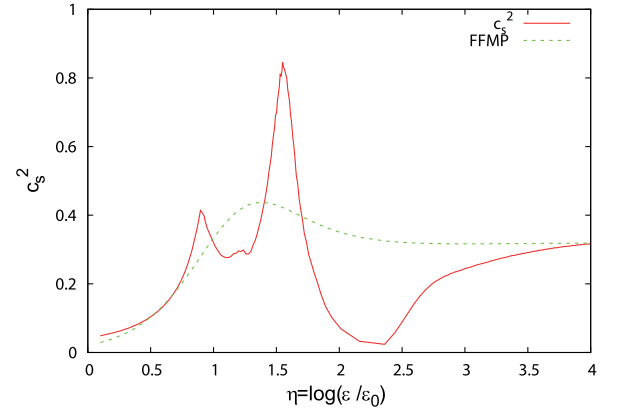

FIG. 23.　The η dependence of c_s^2 with the baryon volume (34). The solid and dashed lines show the result of our hybrid model and the result obtained by parametrization (7) in Ref. [9], respectively.

We see that Fig. 23 also resembles Fig. 20. In this meaning, the qualitative properties of the thermodynamic quantities do not depend on the detailed description of v_B.

IV. SUMMARY

In summary, in this paper, the simple phenomenological hybrid model with the EVE of baryons and the chiral dynamics is investigated. In the model, we combine the Nambu–Jona-Lasinio model and the hadron resonance gas model. The model interpolates between nuclear matter at saturation density and quark matter at high density. The EOS approaches that of pure quark matter as the density increases. There is the intermediate phase, which is difficult to be identified as a pure hadron phase or a pure quark phase. The speed of sound has a double-peak structure. One peak is related to the EVE of baryons, and the other is related to the hadron-quark transition and the chiral symmetry restoration. If the baryon volume v_B approaches $\frac{3}{n_q}$ gradually, the hadron-quark transition is a typical crossover transition, where n_q is the quark number density of the pure quark phase. If the baryon volume v_B approaches $\frac{3}{n_q}$ abruptly, the first-order-like transition can occur in cooperation with the rapid chiral symmetry restoration, and the speed of sound can be very large.

It seems that the density dependence of the baryon volume is very important for EOS at zero temperature. It is desirable to determine the dependence in the framework of the lattice QCD simulation. Simulations using the imaginary baryon chemical potential [19–22] may be useful for this purpose; see Refs. [23,24] as an example.

It is interesting to investigate neutron star properties using our hybrid model. However, to extend the model to asymmetric matter, we should know not only the density dependence but also the isospin dependence of the baryon volume. The lattice QCD simulation with imaginary baryon and isospin chemical potentials [25] may be useful to determine the dependence.

Recently, repulsion in nuclear matter is discussed [15,26,27] in the context of quarkyonic matter [28]. In quarkyonic matter, the onset of the quark Fermi sea suppresses baryonic matter [29]. The quarkyonic effective field theory [30,31] is developed and the relation between the quarkyonic phase and EVE is discussed. Although the existence of quarkyonic matter is not explicitly assumed in our simple phenomenological hybrid model, there is some kind of quark-hadron duality and an intermediate phase that cannot be identified as pure hadron matter or pure quark matter appears. The study of the relation between quarkyonic matter and baryon volume may be important.

On the thermal QCD transition, the possibility of the existence of the partial deconfinement phase has been discussed recently; for a recent review, see, e.g., Ref. [32]. The partial deconfinement can be regarded as the coexistence of two phases in the internal color space rather than in the coordinate space. The intermediate phase which appears in our model may also be understood as such a phase.

[1] K. Fukushima and T. Hatsuda, Rep. Prog. Phys. **74**, 014001 (2011).

[2] J. Cleymans, R. V. Gavai, and E. Suhonen, Phys. Rep. **130**, 217 (1986).

[3] J. Cleymans, K. Redlich, H. Satz, and E. Suhonen, Z. Phys. C **33**, 151 (1986).

[4] H. Kouno and F. Takagi, Z. Phys. C **42**, 209 (1989).

[5] D. H. Rischke, M. I. Gorenstein, H. Stoecker, and W. Greiner, Z. Phys. C **51**, 485 (1991).

[6] Y. Fujimoto, K. Fukushima, Y. Hidaka, A. Hiraguchi, and K. Iida, Phys. Lett. B **835**, 137524 (2022).

[7] Y. Nambu and G. Jona-Lasinio, Phys. Rev. **122**, 345 (1961); **124**, 246 (1961).

[8] T. Hatsuda and T. Kunihiro, Phys. Rep. **247**, 221 (1994).

[9] Y. Fujimoto, K. Fukushima, L. D. McLerran, and M. Praszalowicz, Phys. Rev. Lett. **129**, 252702 (2022).

[10] T. Kojo, AAPPS Bull. **31**, 11 (2021).

[11] M. A. Shifman, in *Proceedings of the 8th International Symposium on Heavy Flavor Physics* (World Scientific, Singapore, 2000), Vol. 3, pp. 1447–1494, 10.1142/9789812810458_0032.

[12] P. Rehberg, S. P. Klevansky, and J. Hufner, Phys. Rev. C **53**, 410 (1996).

[13] R. L. Workman *et al.* (Particle Data Group), Prog. Theor. Exp. Phys. **2022**, 083C01 (2022).

[14] K. Masuda, T. Hatsuda, and T. Takatsuka, Prog. Theor. Exp. Phys. **2013**, 073D01 (2013).

[15] K. S. Jeong, L. McLerran, and S. Sen, Phys. Rev. C **101**, 035201 (2020).

[16] A. Barducci, R. Casalbuoni, G. Pettini, and R. Gatto, Phys. Lett. B **301**, 95 (1993).

[17] K. Kashiwa, M. Yahiro, H. Kouno, M. Matsuzaki, and Y. Sakai, J. Phys. G **36**, 105001 (2009).

[18] Y. Sakai, T. Sasaki, H. Kouno, and M. Yahiro, Phys. Rev. D **82**, 076003 (2010).

[19] P. de Forcrand and O. Philipsen, Nucl. Phys. **B642**, 290 (2002).

[20] M. D'Elia and M.-P. Lombardo, Phys. Rev. D **67**, 014505 (2003).

[21] K. Nagata and A. Nakamura, Phys. Rev. D **83**, 114507 (2011).

[22] J. Takahashi, H. Kouno, and M. Yahiro, Phys. Rev. D **91**, 014501 (2015).

[23] A. Roberge and N. Weiss, Nucl. Phys. **B275**, 734 (1986).

[24] K. Kashiwa, Symmetry **11**, 562 (2019).

[25] M. D'Elia and F. Sanfilippo, Phys. Rev. D **80**, 014502 (2009).

[26] L. McLerran and S. Reddy, Phys. Rev. Lett. **122**, 122701 (2019).

[27] D. C. Duarte, S. Hernandez-Ortiz, and K. S. Jeong, Phys. Rev. C **102**, 065202 (2020).

[28] L. McLerran and R. D. Pisarski, Nucl. Phys. **A796**, 83 (2007).

[29] T. Kojo, Phys. Rev. D **104**, 074005 (2021).

[30] D. C. Duarte, S. Hernandez-Ortiz, K. S. Jeong, and L. D. McLerran, Phys. Rev. D **104**, L091901 (2021).

[31] D. C. Duarte, S. Hernandez-Ortiz, K. S. Jeong, and L. D. McLerran, Phys. Rev. C **107**, 065201 (2023).

[32] M. Hanada and H. Watanabe, On thermal transition in QCD, arXiv:2310.07533.